Central Washington University
ScholarWorks@CWU

All Faculty Scholarship for the College of the Sciences

College of the Sciences

2006

Geochronology and Tectonic Significance of Middle Proterozoic Granitic Orthogneiss, North Qaidam HP/UHP Terrane, Western China

Chris G. Mattinson
Stanford University, mattinson@geology.cwu.edu

Joseph L. Wooden
U.S. Geological Survey

Juhn G. Liou
Stanford University

D. K. Bird
Stanford University

C. L. Wu
Institute of Geology, Chinese Academy of Geological Sciences

Follow this and additional works at: http://digitalcommons.cwu.edu/cotsfac

Part of the Geochemistry Commons, Geology Commons, and the Geomorphology Commons

Geochronology and tectonic significance of Middle Proterozoic granitic orthogneiss, North Qaidam HP/UHP terrane, Western China

C.G. Mattinson[1], J.L. Wooden[2], J.G. Liou[1], D.K. Bird[1], and C.L. Wu[3]

[1]Dept. of Geological & Environmental Sciences,

Stanford University, Stanford, CA, U.S.A.

[2]United States Geological Survey, Menlo Park, CA, U.S.A.

[3]Chinese Academy of Geological Sciences,

Institute of Geology, Beijing, China

1

Summary

Amphibolite-facies para- and orthogneisses near Dulan, in the southeast part of the North Qaidam terrane, enclose minor ultra-high pressure (UHP) eclogite and peridotite. Field relations and coesite inclusions in zircons from paragneiss suggest that felsic, mafic, and ultramafic rocks all experienced UHP metamorphism and a common amphibolite-facies retrogression. SHRIMP-RG U-Pb and REE analyses of zircons from two granitic orthogneisses indicate magmatic crystallization at 927 ± 7 Ma and 921 ± 7 Ma. Zircon rims in one of these samples yield younger ages (397–618 Ma) compatible with partial zircon recrystallization during in-situ Ordovician-Silurian eclogite-facies metamorphism previously determined from eclogite and paragneiss in this area. The similarity between a 2496 ± 18 Ma xenocrystic core and 2.4–2.5 Ga zircon cores in the surrounding paragneiss suggests that the granites intruded the sediments or that the granite is a melt of the older basement which supplied detritus to the sediments. The magmatic ages of the granitic orthogneisses are similar to 920–930 Ma ages of (meta)granitoids described further northwest in the North Qaidam terrane and its correlative west of the Altyn Tagh fault, suggesting that these areas formed a coherent block prior to widespread Middle Proterozoic granitic magmatism.

Introduction

Metamorphism at ultra-high pressure (UHP; coesite stability field, P>27 kbar) conditions in continental subduction-collision belts has been documented from more than 15 localities (e.g., *Liou* et al., 2002). Typically, evidence of UHP meta-

morphism is preserved as rare mineral inclusions or relict mineral assemblages within host rocks that equilibrated at crustal conditions. Lower-pressure rocks that predate the UHP metamorphism but preserve pre-UHP mineral assemblages, textures, and isotopic compositions (e.g., *Lappin* et al., 1979; *Tilton* et al., 1997; *Krabbendam* et al., 2000; *Wain* et al., 2001) have been interpreted to indicate either tectonic juxtaposition after UHP metamorphism ("exotic"), or widespread metastability of lower pressure assemblages during in-situ UHP metamorphism (e.g., *Griffin* et al., 1985; *Austrheim*, 1987; *Cong* et al., 2000).

Granitic orthogneiss in the North Qaidam HP/UHP terrane of western China (Fig. 1) encloses eclogite, yet lacks mineralogic evidence of UHP metamorphism. These relations have been interpreted to indicate a metamorphic and tectonic history for the orthogneiss separate from that of the adjacent HP/UHP rocks: *Song* et al. (2003a) proposed that although the orthogneiss may have provided detritus to the protolith of the adjacent, coesite-bearing paragneiss, the orthogneiss itself may not have experienced UHP metamorphism, requiring an "exotic" origin for the eclogite layers enclosed by the orthogneiss. *Gehrels* et al. (2003a) interpreted high-pressure metamorphism to predate granitic intrusion, requiring continental collision during or prior to mid-Proterozoic time rather than in the early Paleozoic as previously proposed (*Song* et al., 2005; *Yang* et al., 2001a, b, c). Here we present SHRIMP-RG U-Pb geochronology and REE geochemistry of zircons from two granitic orthogneisses near Dulan (Fig. 1), in the southeast part of the North Qaidam terrane, to clarify the relation between the orthogneiss and adjacent HP/UHP rocks.

Geologic Background

The northwest-southeast trending North Qaidam terrane records early Paleozoic continental collision, and is bounded on the southwest by the Qaidam Basin, and on the northeast by the Qilian terrane (Fig. 1; *Yang* et al., 2001c). The basement of the North Qaidam terrane is the Proterozoic Dakandaban Group gneiss, which is overlain by Paleozoic metasediments, and intruded by granites. The Dakandaban Group includes paragneiss, orthogneiss, marble, amphibolite, migmatite, and locally eclogite and garnet peridotite (*Yang* et al., 1994, 1998, 2001a, c). Eclogite has been discovered over a distance of 350 km, in the Lüliang Shan, Xitie Shan, and near Dulan (Fig. 1). The eclogite and peridotite occur as blocks, boudins or layers in the host para- and orthogneiss, and typically are 10's to <1m across. Zircon U-Pb ages from gneiss, eclogite, and peridotite of the North Qaidam terrane have been interpreted to record peak metamorphism between 423–497 Ma, similar to Sm-Nd garnet-omphacite-whole rock isochron ages from eclogite (*Yang* et al., 2001b, c, 2002; *Song* et al., 2003a, 2005; *Zhang* et al., 2005b).

The granites cross-cut the regional foliation; they crystallized between 397–456 Ma, and are thought to be coeval with continental collision between the North Qaidam and Qilian terranes (*Gehrels* et al., 2003a; *Wu* et al., 2001, 2004). North of the North Qaidam terrane, granites in the southern Qilian terrane (Fig. 1) have I-type geochemistry, 425–496 Ma ages, and are interpreted to represent arc magmatism (*Gehrels* et al., 2003a; *Wu* et al., 2001). The subduction polarity responsible for convergence, magmatism, and subsequent collision of the North Qaidam and Qilian terranes is unclear, and models involving both north-dipping subduction (*Yang* et al., 2001c, 2002; *Yin* and *Harrison*, 2000) and south-dipping

subduction (*Gehrels* et al., 2003a, b) have been proposed. Additional field and geochronological work is required to resolve this problem.

Near Dulan, collision-related granite and granodiorite of the Yematan batholith (Fig. 2) cut the northwest striking amphibolite-facies foliation in the Dakandaban Group gneisses, and yield a U-Pb zircon age of 397 ± 3 Ma (*Wu* et al., 2001, 2004). *Song* et al. (2003b) determined peak conditions of 631–746°C, 29–33 kbar for eclogites near Dulan, and the discovery of coesite included in zircon from the host paragneiss confirms that both the mafic/ultramafic rocks and the felsic host gneiss were metamorphosed at UHP conditions (*Song* et al., 2001a, b, 2003b; *Yang* et al., 2001a). Our recent zircon U-Pb geochronology from paragneiss, eclogite, and amphibolite near Dulan indicate eclogite-facies metamorphism at 450–425 Ma (*Mattinson* et al., 2004, 2005). Zircon U-Pb ages of 932–1097 Ma have been reported for granitic orthogneiss in the Dulan area (*Song* et al., 2001a, b; *Yang* et al., 2001b). All rock types were subsequently uplifted and eroded during Cenozoic deformation associated with the India-Asia collision.

Sample Description

Two samples of granitic orthogneiss were collected for zircon U-Pb geochronology (Fig. 2). Both samples are medium-grained, with a well-developed foliation defined by muscovite and biotite, concordant with the fabric in the surrounding rocks. Granitic orthogneiss D7B contains quartz, microcline, sericitized plagioclase, muscovite, biotite, apatite, very minor garnet, and zircon. The sample (collected at N36°31.07′, E98°36.75′) is adjacent to a ∼1km-long, variably serpentinized peridotite, which contains layers of garnet clinopyroxenite. Small layers

of garnet amphibolite preserving eclogite relics occur within the orthogneiss and the adjacent paragneiss. Granitic orthogneiss D15D contains quartz, microcline, plagioclase, minor muscovite, biotite, apatite, very minor garnet, tourmaline, and zircon. The sample (collected at N36°35.94′, E98°28.45′) is adjacent to several eclogite and amphibolite layers.

Analytical Methods

Zircon U-Pb geochronology and trace element analyses were performed in separate analytical sessions using the Stanford/USGS SHRIMP-RG (reverse geometry) facility. Zircon grains separated from the samples were mounted with zircon age standard R33 (*Black* et al., 2004) in a 2.54 cm epoxy disc and polished to approximate half-sections prior to reflected light and cathodoluminescence (CL) imaging. Cathodoluminescence images were collected using a JEOL 5600LV scanning electron microscope equipped with a Hamamatsu photomultiplier tube. SHRIMP analysis spots were chosen to avoid any cracks, pits, or inclusions identified in CL and reflected light images. The sample was coated with high-purity Au, and placed under high vacuum for one day prior to analysis to minimize interference from gas species.

The analytical routine for U-Pb geochronology followed *Williams* (1998), and age calculations were performed using the Isoplot and Squid programs (*Ludwig*, 2001, 2003) and IUGS recommended decay constants (*Steiger* and *Jäger*, 1977). The sample was sputtered by a $\sim$5 nA O_2^- primary beam focused to $\sim$30 μm diameter, and the mass resolution was 6000–7000 at 10% peak height. Prior to analysis, the primary ion beam was rastered across the grain surface to remove

6

the Au-coating and any surface contamination. For each analysis, 5–6 scans of peaks corresponding to $^{90}Zr_2^{16}O$, ^{204}Pb, background, ^{206}Pb, ^{207}Pb, ^{208}Pb, ^{238}U, $^{232}Th^{16}O$ and $^{238}U^{16}O$ were collected, with count times of 2–16 s for each peak. The concentration of U was calibrated using zircon standard CZ3 (U = 550 ppm; *Pidgeon* et al., 1994), and the Pb/U ratio was calibrated using zircon age standard R33 (419 Ma; *Black* et al., 2004). Zircons from the samples were analyzed over two sessions: three analyses of each sample were conducted in a reconnaissance session (not included in Fig. 3 or concordia age calculations) for which the R33 $^{206}Pb/^{238}U$ calibration error was 0.46% (2σ; Table 1); the remaining analyses were conducted in a second session for which the R33 $^{206}Pb/^{238}U$ calibration error was 0.66% (2σ; Table 1). Common Pb compositions were estimated using the two-stage Pb evolution model of *Stacey* and *Kramers* (1975).

For trace element analyses, we selected one isotope to represent each element, based on abundance and absence of significant interferences, similar to the approach of *Maas* et al. (1992). Peaks selected were: $^{28}Si^{16}O_2$, ^{96}Zr, ^{139}La, ^{140}Ce, ^{141}Pr, ^{144}Nd, ^{147}Sm, ^{151}Eu, ^{157}Gd, ^{163}Dy, $^{166}Er^{16}O$, $^{172}Yb^{16}O$, $^{175}Lu^{16}O$, $^{180}Hf^{16}O$, ^{232}Th, and ^{238}U. Operating at $\sim$10,000 mass resolution at 10% peak height, these peaks are well resolved from LREE oxides and Zr, Si, O molecules, but due to an unresolved ^{140}CeH interference on ^{141}Pr, Pr abundances are not included in Fig. 3 and Table 2. Primary beam current and spot size were similar to those used for geochronology. A complete analysis of four scans, with count times of 8 s for the LREE, 4 s for the HREE, Th, and U, and 2 s for Si, Zr, and Hf takes approximately 15 minutes, including the time required for peak centering and magnet settling. After every five unknowns, NIST SRM 611 and SRM 613 glasses (*Pearce* et al., 1997) were analyzed to monitor instrument stability. Sri Lankan gem zircon

SL13 was analyzed as a concentration standard. The raw data were converted to ppm by normalizing average count rates to silicon, correcting for natural isotopic abundance, and calibrating concentrations to trace element values for zircon standard SL13 reported by *Hoskin* (1998). These concentrations were converted to chondrite-normalized patterns (*Coryell* et al., 1963) using the recommended composition for CI carbonaceous chondrites of *McDonough* and *Sun* (1995).

Geochronology, chondrite-normalized REE patterns, and representative CL images of zircons from two orthogneisses (sample locations shown in Fig. 2) are described below and are shown in Fig. 3. Individual ages reported below are ^{206}Pb/^{238}U ages corrected for common Pb using ^{207}Pb (*Williams*, 1998) unless otherwise noted. Ages calculated from multiple analyses are expressed as concordia ages (*Ludwig*, 1998) corrected for common Pb using ^{204}Pb, and errors are given at 95% confidence. The concordia age utilizes all radiogenic Pb/U and Pb/Pb ratios, and provides a quantitative assessment of both equivalence and concordance, and is therefore a more rigorous statistical treatment of the data than a weighted mean of ^{206}Pb/^{238}U ages alone (*Ludwig*, 1998).

Results

Most zircons from granitic orthogneiss D7B display oscillatory zoning in CL (Fig. 3c, analyses 5 and 19), with or without a dark CL core (Fig. 3c, analysis 14), and several grains contain a luminous, unzoned rim (Fig. 3c, analyses 3 and 10). Sixteen analyses of the oscillatory zoned interior yield 386–1392 ppm U, and Th/U = 0.06–0.53 (Fig. 3e; Table 1). The concordia age (*Ludwig*, 1998) of 926.6 ± 6.9 Ma (from nine analyses; Fig. 3a; Table 1) excludes three analyses with minor reverse

discordance, and younger analyses which we interpret to have experienced Pb-loss. The chondrite-normalized REE patterns (Fig. 3c) contain prominent negative Eu anomalies [Eu/Eu* $= \text{Eu}_n/(\text{Sm}_n \times \text{Gd}_n)^{0.5} = 0.02$–$0.16$; the subscript indicates chondrite normalization to the values of *McDonough* and *Sun* (1995)], and are enriched in HREE ($\text{Lu}_n = 1000$–4400; Fig. 3c and Table 2), consistent with magmatic zircon co-crystallized with feldspar. Several core analyses that yield younger ages contain slightly elevated common Pb levels (Fig. 3a; Table 1, analyses 2, 9, and 20) compared to the other analyses. Analyses of the luminous rims (Fig. 3c, analyses 3 and 10) yield 397–618 Ma ages, 175–408 ppm U, Th/U $= 0.006$–0.06, and slightly elevated common Pb levels compared with the oscillatory-zoned interiors (Figs. 3b and e; Table 1). Trace element analyses of two rims contain less pronounced Eu anomalies, flatter LREE slopes, and lower HREE concentrations (Eu/Eu* $=$ 0.16–0.33, $\text{Lu}_n = 100$–1000; Fig. 3c and Table 2, analyses 1 and 3).

The zircons from granitic orthogneiss D15D display euhedral, oscillatory CL zoning, with brighter CL euhedral cores surrounded by darker CL rims (Fig. 3f, analyses 1, 2, and 5), without obvious metamorphic overgrowths. Seventeen analyses yield 115–1418 ppm U (increasing from core to rim), and Th/U $= 0.07$–0.45 (Fig. 3e; Table 1). The concordia age (*Ludwig*, 1998) of 921.4 ± 7.0 Ma (from 11 analyses; Fig. 3d; Table 1) excludes younger analyses which we interpret to have experienced Pb-loss. The REE patterns contain prominent negative Eu anomalies (Eu/Eu* $= 0.06$–0.20), and are enriched in HREE ($\text{Lu}_n = 600$–6900; Fig. 3f and Table 2), similar to D7B. Several analyses that yield younger ages contain slightly elevated common Pb levels (Fig. 3d; Table 1, analyses 5, 6, and 13), and a REE pattern of one analysis (Fig. 3f, analysis 5; Table 2) contains elevated LREE and a flatter LREE slope compared to the other analyses. A few grains contain

bright CL, rounded cores; analysis of one core (Fig. 3f, analysis 17; Table 1) yields a slightly discordant 2496 $\pm$ 18 Ma ^{207}Pb/^{206}Pb age (corrected for common Pb using measured ^{204}Pb).

Discussion

We interpret orthogneiss samples D7B and D15D to record magmatic crystallization at 926.6 $\pm$ 6.9 Ma and 921.4 $\pm$ 7.0 Ma, respectively, based on euhedral oscillatory zoning in CL (e.g., *Hanchar* and *Miller*, 1993; *Corfu* et al., 2003), Th/U ratios (e.g., *Williams* et al., 1996; *Mojzsis* and *Harrison*, 2002; *Rubatto*, 2002; *Hoskin* and *Schaltegger*, 2003; but see also *Möller* et al., 2002), and REE patterns (e.g., *Maas* et al., 1992; *Schaltegger* et al., 1999; *Rubatto*, 2002; *Hoskin* and *Schaltegger*, 2003; *Whitehouse* and *Kamber*, 2003). This interpretation is consistent with sparse muscovite, biotite, and plagioclase inclusions in zircon, identified by electron microprobe. The prominent negative Eu-anomalies (Figs. 3c and f; Table 2) are typical of zircon equilibrated with feldspar, even in the absence of a whole-rock Eu anomaly (*Rubatto*, 2002; *Rubatto* and *Hermann*, 2003), due to the preferential incorporation of Eu in feldspar (*Philpotts* and *Schnetzler*, 1968).

We interpret younger analyses of the oscillatory zoned cores to have been affected by Pb-loss, so they are not included in the calculation of the concordia ages. Several of the younger ages are marked by slightly elevated common Pb levels, and one REE analysis shows elevated LREE (Fig. 3c and Table 2, analysis D15D-5). Elevated zircon LREE has been attributed to growth or alteration under hydrothermal conditions, and LREE incorporation may be enhanced by radiation damage (e.g., *Maas* et al., 1992; *Whitehouse* and *Kamber*, 2002; *Hoskin*,

2005; *Rayner* et al., 2005). Elevated common Pb may also be incorporated in zircon during hydrothermal growth or alteration (*Watson* et al., 1997; *Rayner* et al., 2005). We therefore suggest that similar processes, probably accompanying Ordovician-Silurian metamorphism, may be responsible for the Pb-loss observed in our samples.

Analyses of the high CL rims in sample D7B do not yield a coherent age group, in part due to minor overlap with cores, complicated by elevated common Pb levels. The ages are similar to 425–450 Ma zircon ages of eclogite-facies metamorphism in adjacent eclogite and paragneiss (*Mattinson* et al., 2004, 2005), suggesting that zircon rims in orthogneiss formed during the same event. As noted above, the flat LREE patterns and elevated common Pb levels may indicate that rims formed by fluid-mediated growth or recrystallization (e.g., *Maas* et al., 1992; *Watson* et al., 1997; *Whitehouse* and *Kamber*, 2002; *Hoskin*, 2005; *Rayner* et al., 2005). The euhedral external crystal faces (Fig. 3c) are compatible with either recrystallization of preexisting zircon or resorption followed by new growth.

The luminous CL rims of sample D7B contain variable Th/U ratios lower than those in the oscillatory zoned cores (Fig. 3d; Table 1). Metamorphic recrystallization of zircon releases trace elements such as U, Th, Pb, and REE, and the less compatible Th will be expelled preferentially relative to U (*Pidgeon*, 1992; *Pidgeon* et al., 1998; *Hoskin* and *Black*, 2000). The Th/U ratio is commonly used as a discriminant between igneous and metamorphic zircon, but this criterion must be applied cautiously, as low Th/U may also result from fluid composition or coexisting Th-rich minerals (*Keppler* and *Wyllie*, 1990; *Hermann*, 2002). In this case, the variable Th/U is best explained by incomplete recrystallization. The analysis with the lowest Th/U ratio also has the lowest REE concentration (analysis

11

3), consistent with a recrystallization origin (*Pidgeon*, 1992; *Pidgeon* et al., 1998; *Hoskin* and *Black*, 2000). The low HREE concentration in analysis 3 may also reflect equilibration with minor garnet in the sample (e.g., *Schaltegger* et al., 1999; *Rubatto*, 2002; *Whitehouse* and *Platt*, 2003).

The ages we obtain are similar to previously reported 932–1097 Ma orthogneiss ages from the Dulan area (*Song* et al., 2001a, b; *Yang* et al., 2001b). However, based on the absence of metamorphic overgrowths visible in CL, *Song* et al. (2003a) concluded that the Dulan orthogneiss may not have experienced UHP metamorphism. The metamorphic rims in sample D7B (Fig. 3c, analyses 3 and 10; Table 1) support our conclusion, based on field evidence, that both para- and orthogneisses share a common metamorphic history, including UHP metamorphism. *Song* et al. (2003a) also concluded, based on the similarity between CL textures in paragneiss detrital cores and orthogneiss grains, that the orthogneiss may be a source for the sedimentary protolith of the paragneiss. However, the presence of a 2496 ± 18 Ma xenocrystic core in one orthogneiss zircon (Fig. 3c, analysis 17), similar in age to zircon detrital cores in adjacent paragneiss, suggests that the granite intruded the sediments or that the granite is a melt of the older basement which supplied detritus to the sediments. Of 15 paragneiss grain cores analyzed, 5 are 2.4–2.5 Ga, including 3 analyses that are <10% discordant, and the youngest analysis <30% discordant is 1.45 Ga; no 920–930 Ma ages were obtained (*Mattinson* et al., 2004, 2005, unpubl. data).

Middle Proterozoic (meta)granitic plutons similar in age to those presented in this study have been described to the north, in the Qilian terrane (*Gehrels* et al., 2003a), to the northwest, in the Lüliang Shan (*Gehrels* et al., 2003a; *C.A. Menold*, pers. commun., 2005; *J.X. Zhang*, pers. commun., 2005), and northwest

of the Altyn Tagh fault, near Xorkol (*Gehrels* et al., 2003a, b), and near Bashiwake (*C.G. Mattinson* and *J.X. Zhang*, unpubl. data; for locations see Fig. 1). These data support the conclusion of *Gehrels* et al. (2003a, b) that much of the North Qaidam and Qilian terranes, and their presumed western extensions across the Altyn Tagh fault formed a coherent crustal fragment by Middle Proterozoic time.

Acknowledgements

References

Austrheim H (1987) Eclogitization of lower crustal granulites by fluid migration through shear zones. Earth Planet Sci Lett 81: 221-232

Black LP, Kamo SL, Allen CM, Davis DW, Aleinikoff JN, Valley JW, Mundil R, Campbell IH, Korsch RJ, Williams IS, Foudoulis C (2004) Improved ^{206}Pb/^{238}U microprobe geochronology by the monitoring of a trace-element-related matrix effect; SHRIMP, ID-TIMS, ELA-ICP-MS and oxygen isotope documentation for a series of zircon standards. Chem Geol 205: 115-140

Cong B, Wang Q, Zhai M (2000) New data regarding hotly debated topics concerning UHP metamorphism of the Dabie-Sulu belt, east-central China. In: Ernst WG, Liou JG (eds) Ultra-high pressure metamorphism and geodynamics in collision-type orogenic belts. Bellwether Publishing, Columbia, pp 181-189

Corfu F, Hanchar JM, Hoskin PWO, Kinny P (2003) Atlas of Zircon Textures. Rev Mineral Geochem 53: 469-500

Coryell CD, Chase JW, Winchester JW (1963) A procedure for geochemical interpretation of terrestrial rare-earth abundance patterns. J Geophys Res 68: 559-566

Gehrels GE, Yin A, Wang X-F (2003a) Magmatic history of the northeastern Tibetan Plateau. J Geophys Res 108: 2423, doi:2410.1029/2002JB001876

Gehrels GE, Yin A, Wang X-F (2003b) Detrital-zircon geochronology of the northeastern Tibetan plateau. Geol Soc Am Bull 115: 881-896

Griffin WL, Austrheim H, Brastad K, Bryhni I, Krill AG, Krogh EJ, Mørk MBE, Qvale H, Tørudbakken B (1985) High-pressure metamorphism in the Scandinavian Caledonides. In: Gee DG, Sturt BA (eds) The Caledonide Orogen— Scandinavia and Related Areas. Wiley, New York, pp 783-801

Hanchar JM, Miller CF (1993) Zircon zonation patterns as revealed by cathodoluminescence and backscattered electron images: Implications for interpretation of complex crustal histories. Chem Geol 110: 1-13

Hermann J (2002) Allanite: thorium and light rare earth element carrier in subducted crust. Chem Geol 192: 289-306

Hoskin PWO (1998) Minor and trace element analysis of natural zircon ($ZrSiO_4$) by SIMS and laser ablation ICPMS: A consideration and comparison of two

broadly competitive techniques. J Trace Microprobe T 16: 301-326

Hoskin PWO (2005) Trace-element composition of hydrothermal zircon and the alteration of Hadean zircon from the Jack Hills, Australia. Geochim Cosmochim Ac 69: 637-648

Hoskin PWO, Black LP (2000) Metamorphic zircon formation by solid-state recrystallization of protolith igneous zircon. J Metamorph Geol 18: 423-439

Hoskin PWO, Schaltegger U (2003) The composition of zircon and igneous and metamorphic petrogenesis. Rev Mineral Geochem 53: 27-62

Keppler H, Wyllie PJ (1990) Role of fluids in transport and fractionation of uranium and thorium in magmatic processes. Nature 348: 531-533

Krabbendam M, Wain A, Andersen TB (2000) Pre-Caledonian granulite and gabbro enclaves in the Western Gneiss Region, Norway: indications of incomplete transition at high pressure. Geol Mag 137: 235-255

Lappin MA, Pidgeon RT, van Breemen O (1979) Geochronology of basal gneisses and mangerite syenites of Stadlandet, west Norway. Norsk Geol Tidsskr 59: 161-181

Liou JG, Zhang RY, Katayama I, Maruyama S (2002) Global distribution and petrotectonic characterizations of UHPM terranes. In: Parkinson CD, Katayama I, Liou JG, Maruyama S (eds) The diamond-bearing Kokchetav massif, Kazakhstan. Universal Academy Press, Tokyo, Japan, pp 15-35

Ludwig KR (1998) On the treatment of concordant uranium-lead ages. Geochim Cosmochim Ac 62: 665-676

Ludwig KR (2001) Squid 1.02: A user's manual, Berkeley Geochronology Center Special Publication No. 2, pp 1-19

Ludwig KR (2003) User's manual for Isoplot 3.00: A geochronological toolkit for Microsoft Excel, Berkeley Geochronology Center Special Publication No. 4, pp 1-70

Maas R, Kinny PD, Williams IS, Froude DO, Compston W (1992) The Earth's oldest known crust: A geochronological and geochemical study of 3900–4200 Ma detrital zircons from Mt. Narryer and Jack Hills, Western Australia. Geochim Cosmochim Ac 56: 1281-1300

Mattinson CG, Liou JG, Bird DK, Wooden JL, Wu CL, Yang JS (2004) Geochronology and mineral inclusions of eclogite, ortho-, and paragneiss zircon, North Qaidam UHP terrane, northwest China. Eos Trans AGU 85: F1656

Mattinson CG, Liou JG, Bird DK, Wooden JL, Wu C, Yang J (2005) Zircon geochronology and REE geochemistry, North Qaidam UHP terrane, northwest China. Mitt Österr Miner Ges 150: 106

McDonough WF, Sun S-s (1995) The composition of the Earth. Chem Geol 120: 223-253

Mojzsis SJ, Harrison TM (2002) Establishment of a 3.83-Ga magmatic age for the Akilia tonalite (southern West Greenland). Earth Planet Sci Lett 202(3-4): 563-576

Möller A, O'Brien PJ, Kennedy A, Kröner A (2002) Polyphase zircon in ultrahigh–temperature granulites (Rogaland, SW Norway): constraints for Pb diffusion in zircon. J Metamorph Geol 20: 727-740

Pearce NJG, Perkins WT, Westgate JA, Gorton MP, Jackson SE, Neal CR, Chenery SP (1997) A compilation of new and published major and trace element data for NIST SRM 610 and NIST SRM 612 glass reference materials. Geostandard Newslett 21: 115-144

Philpotts JA, Schnetzler CC (1968) Europium anomalies and the genesis of basalt. Chem Geol 3: 5-13

Pidgeon RT (1992) Recrystallisation of oscillatory zoned zircon: some geochronological and petrological implications. Contrib Mineral Petr 110: 463-472

Pidgeon RT, Furfaro D, Kennedy AK, Nemchin AA, van Bronswjk W (1994) Calibration of zircon standards for the Curtin SHRIMP II. US Geol Surv Circ 1107: 251

Pidgeon RT, Nemchin AA, Hitchen GJ (1998) Internal structures of zircons from Archaean granites from the Darling Range batholith: implications for zircon stability and the interpretation of zircon U-Pb ages. Contrib Mineral Petr 132: 288-299

Rayner N, Stern RA, Carr SD (2005) Grain-scale variations in trace element composition of fluid-altered zircon, Acasta Gneiss Complex, northwestern Canada. Contrib Mineral Petr 148(6): 721-734

Rubatto D (2002) Zircon trace element geochemistry: partitioning with garnet and the link between U-Pb ages and metamorphism. Chem Geol 184: 123-138

Rubatto D, Hermann J (2003) Zircon formation during fluid circulation in eclogites (Monviso, Western Alps): Implications for Zr and Hf budget in subduction zones. Geochim Cosmochim Ac 67: 2173-2187

Schaltegger U, Fanning CM, Günther D, Maurin JC, Schulmann K, Gebauer D (1999) Growth, annealing and recrystallization of zircon and preservation of monazite in high-grade metamorphism: conventional and in-situ U-Pb isotope, cathodoluminescence and microchemical evidence. Contrib Mineral Petr 134: 186-201

Song S, Yang J, Katayama I, Liu F, Maruyama S (2001a) Zircons and their inclusions from various rocks in the Dulan UHP metamorphic terrane, the North Qaidam, NW China. In: UHPM workshop 2001: Fluid/slab/mantle interactions and ultrahigh-P minerals. Waseda University, Tokyo, Japan, pp 116-120

Song S, Yang J, Liou JG, Wu C, Shi R, Xu Z (2003a) Petrology, geochemistry and isotopic ages of eclogites from the Dulan UHPM terrane, the North Qaidam, NW China. Lithos 70: 195-211

Song S, Yang J, Wu C, Liou JG, Xu Z (2001b) Petrology, geochemistry, and isotopic ages of eclogites in the Dulan UHPM terrane, the North Qaidam, NW China. In: Sixth International Eclogite Conference, Niihama, Japan, p 150

Song S, Zhang L, Niu Y, Su L, Jian P, Liu D (2005) Geochronology of diamond-bearing zircons from garnet peridotite in the North Qaidam UHPM belt, Northern Tibetan Plateau: A record of complex histories from oceanic lithosphere subduction to continental collision. Earth Planet Sci Lett 234: 99-118

Song SG, Yang JS, Xu ZQ, Liou JG, Shi RD (2003b) Metamorphic evolution of the coesite-bearing ultrahigh-pressure terrane in the North Qaidam, Northern Tibet, NW China. J Metamorph Geol 21: 631-644

Stacey JS, Kramers JD (1975) Approximation of terrestrial lead isotope evolution by a two-stage model. Earth Planet Sci Lett 26: 207-221

Steiger RH, Jäger E (1977) Subcommission on geochronology: Convention on the use of decay constants in geo- and cosmochemistry. Earth Planet Sci Lett 36: 359-362

Tera F, Wasserburg GJ (1972) U-Th-Pb systematics in three Apollo 14 basalts and the problem of initial Pb in lunar rocks. Earth Planet Sci Lett 14: 281-304

Tilton GR, Ames L, Schertl H-P, Schreyer W (1997) Reconnaissance isotopic investigations on rocks of an undeformed granite contact within the coesite-bearing unit of the Dora Maira Massif. Lithos 41: 25-36

Wain AL, Waters DJ, Austrheim H (2001) Metastability of granulites and processes of eclogitisation in the UHP region of western Norway. J Metamorph Geol 19: 609-625

Watson EB, Cherniak DJ, Hanchar JM, Harrison TM, Wark DA (1997) The incorporation of Pb into zircon. Chem Geol 141: 19-31

Wetherill GW (1956) Discordant uranium-lead ages, I. Trans Am Geophys U 37: 320-326

Whitehouse MJ, Kamber BS (2002) On the overabundance of light rare earth elements in terrestrial zircons and its implication for Earth's earliest magmatic differentiation. Earth Planet Sci Lett 204: 333-346

Whitehouse MJ, Kamber BS (2003) A rare earth element study of complex zircons from early Archaean Amîtsoq gneisses, Godthåbsfjord, south-west Greenland. Precambrian Research 126(3-4): 363-377

Whitehouse MJ, Platt JP (2003) Dating high-grade metamorphism–constraints from rare-earth elements in zircon and garnet. Contrib Mineral Petr 145: 61-74

Williams IS (1998) U-Th-Pb geochronology by ion microprobe. In: McKibben MA, Shanks WC, III, Ridley WI (eds) Reviews in Economic Geology Vol 7: Applications of microanalytical techniques to understanding mineralizing

processes. Society of Economic Geologists, pp 1-35

Williams IS, Buick IS, Cartwright I (1996) An extended episode of early Meso-proterozoic metamorphic fluid flow in the Reynolds Range, central Australia. J Metamorph Geol 14(1): 29-47

Wu C, Yang J, Wooden J, Ernst WG, Liou JG, Li H, Zhang J, Wan Y, Shi R (2001) Relationship between UHP eclogite and two different types of granite in the North Qaidam, NW China: Evidence from zircon SHRIMP ages of granites. Eos Trans AGU 82: Abstract V32C-0980

Wu C, Yang J, Wooden JL, Shi R, Chen S, Meibom A, Mattinson C (2004) Zircon U-Pb SHRIMP dating of the Yematan Batholith in Dulan, north Qaidam, NW China. Chinese Sci Bull 49: 1736-1740

Yang J, Song S, Xu Z, Wu C, Mattinson C, Bian A, Zhang RY, Liou JG, Ernst WG (2001a) Northern Qaidam Caledonian UHP terrane: A new discovery. Eos Trans AGU 82: F1342

Yang J, Wu C, Zhang J, Song S, Ireland TR (2001b) U-Pb/Sm-Nd/Ar-Ar ages of the North Qaidam ultrahigh-high pressure metamorphic rocks, NW China. In: Sixth International Eclogite Conference., Niihama, Japan, p 178

Yang J, Xu Z, Zhang J, Chu C-Y, Zhang R, Liou J-G (2001c) Tectonic significance of Early Paleozoic high-pressure rocks in Altun–Qaidam–Qilian Mountains, NW China. Geol Soc Am Mem 194: 151-170

Yang J, Xu Z, Zhang J, Song S, Wu C, Shi R, Li H, Brunel M (2002) Early Paleozoic North Qaidam UHP metamorphic belt on the north-eastern Tibetan plateau and a paired subduction model. Terra Nova 14: 397-404

Yang JJ, Zhu H, Deng JF, Zhou TZ, Lai SC (1994) Discovery of garnet-peridotite at the northern margin of the Qaidam basin and its significance. Acta Petro-

logica et Mineralogica 13: 97-105 (in Chinese with English abstract)

Yang JS, Xu ZQ, Li HB, Wu CL, Cui JW, Zhang JX, Chen W (1998) Discovery of eclogite at northern margin of Qaidam basin, NW China. Chinese Sci Bull 43: 1755-1760 (in Chinese with English abstract)

Yin A, Harrison TM (2000) Geologic evolution of the Himalayan-Tibetan orogen. Ann Rev Earth Planet Sci 28: 211-280

Zhang JX, Mattinson CG, Meng FC, Wan YS (2005a) An Early Palaeozoic HP/HT granulite-garnet peridotite association in the south Altyn Tagh, NW China: P-T history and U-Pb geochronology. J Metamorph Geol 23: 491-510

Zhang JX, Yang JS, Mattinson CG, Xu ZQ, Meng FC, Shi RD (2005b) Two contrasting eclogite cooling histories, North Qaidam HP/UHP terrane, western China: Petrological and isotopic constraints. Lithos 84: 51-76

Authors' addresses: *C. G. Mattinson* (corresponding author; e-mail: cgm@pangea. stanford.edu), *J. G. Liou*, and *D. K. Bird*, Department of Geological & Environmental Sciences, Stanford University, Stanford, California 94305-2115, U.S.A.; *J. L. Wooden*, United States Geological Survey, 345 Middlefield Road, Menlo Park, California 94025, U.S.A.; *C. L. Wu*, Chinese Academy of Geological Sciences, Institute of Geology, Beijing 100037, China.

Figure Captions

Fig. 1. (a) Map of China showing the location of this study (box) and the trends of major mountain belts (dashed lines). (b) Schematic map of the Qaidam-Qilian-Altyn Tagh region showing major tectonic units, and locations of eclogite and garnet peridotite. The box near Dulan (lower right corner) indicates the location

of Fig. 2. Abbreviations: E. Pz, early Paleozoic; Pt, Proterozoic; Ar, Archean. Ages of Proterozoic (meta)granites are from *Gehrels* et al. (2003a, b), except the Bashiwake age, from C.G Mattinson and J.X. Zhang, unpubl. data. Modified from *Zhang* et al. 2005a.

Fig. 2. Geologic sketch map of the study area showing sample locations. Foliation in the Dakandaban Group is dominantly northwest striking, steeply northeast dipping, locally modified by tight, northwest plunging folds. Granite and granodiorite are part of the Yematan batholith (397 ± 3 Ma; *Wu* et al., 2004). The town of Dulan is approximately 30 km southwest of map area. Modified from *Song* et al. (2003a) and *Wu* et al. (2004).

Fig. 3. (a) Tera-Wasserburg concordia (*Tera* and *Wasserburg*, 1972) for sample D7B. Plotted ratios are uncorrected for common Pb, and error ellipses are 2σ. (b) Wetherill concordia (*Wetherill*, 1956) for sample D7B. Plotted ratios are corrected for common Pb using measured ^{204}Pb, and error ellipses are 2σ. (c) Cathodoluminescence images and REE plots (*Coryell* et al., 1963) normalized to chondrite values of *McDonough* and *Sun* (1995) for sample D7B. Circles show the locations of $\sim 30\mu$m SHRIMP-RG analyses, labeled with their analysis number (Tables 1 and 2) and ^{207}Pb-corrected ^{206}Pb/^{238}U age (*Williams*, 1998), and errors are 1σ. (d) Tera-Wasserburg concordia (*Tera* and *Wasserburg*, 1972) for sample D15D.

Plotted ratios are uncorrected for common Pb, and error ellipses are 2σ. (e) Th and U concentration data determined during U-Pb geochronology (Table 1) for samples D7B (filled squares) and D15D (open circles). (f) Cathodoluminescence images and REE plots (*Coryell* et al., 1963) normalized to chondrite values of *Mc-Donough* and *Sun* (1995) for sample D15D. Circles show the locations of $\sim$30μm SHRIMP-RG analyses, labeled with their analysis number (Tables 1 and 2) and ^{207}Pb-corrected ^{206}Pb/^{238}U age (*Williams*, 1998) for ages <1Ga, or ^{204}Pb-corrected ^{207}Pb/^{206}Pb age for ages >1Ga, and errors are 1σ.
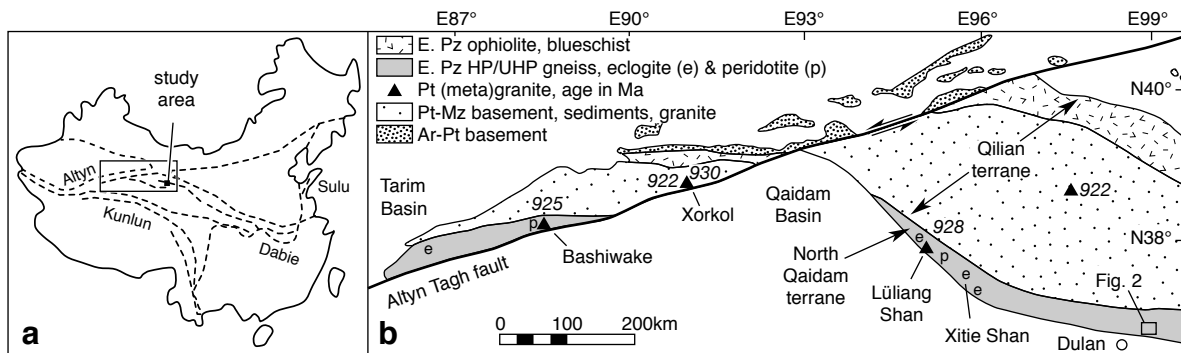
Fig. 1, Mattinson et al.

Fig. 2, Mattinson et al.

a D7B

Concordia age = 926.6 ± 6.9 (95% conf.) on 9 points. Probability of equivalence = 0.94 (MSWD=0.52) Probability of concordance = 0.061

b D7B

cores

rims

c D7B

933±10 874±3

618±8

421±3 936±11

d D15D

Concordia age = 921.4 ± 7.0 (95% conf.) on 11 points. Probability of equivalence = 0.3 (MSWD = 1.1) Probability of concordance = 0.095

e

D7B cores

D15D

Th/U=1

Th/U=0.1

Th/U=0.01

D7B rims

f D15D

2496±18

912±4 897±12

867±10
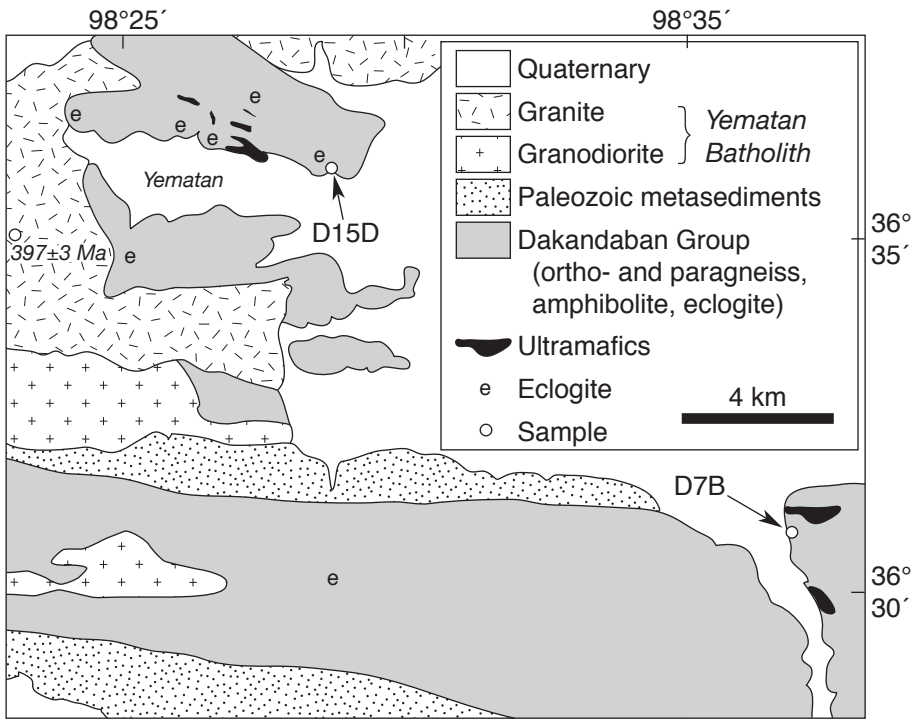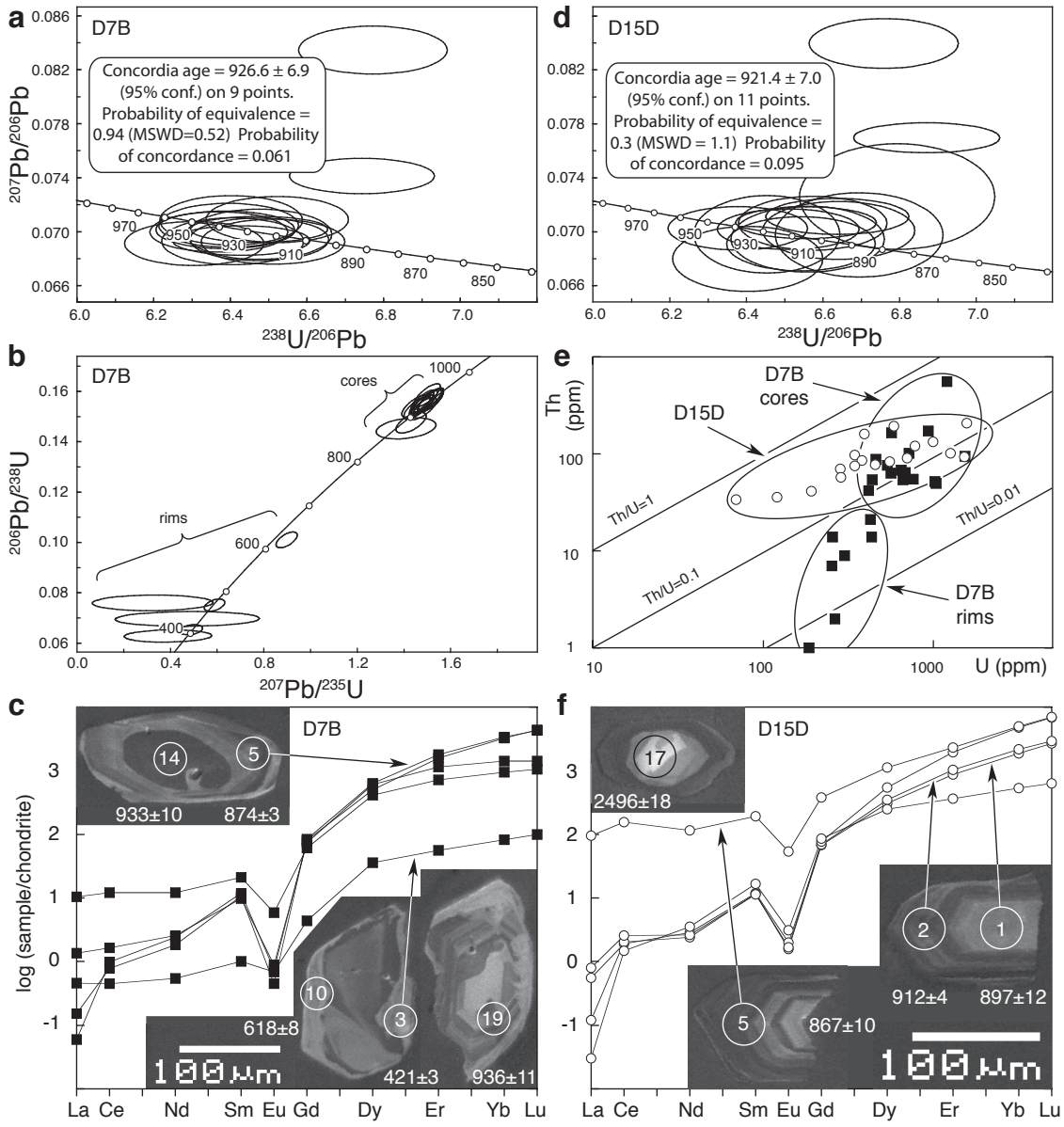
Fig. 3, Mattinson et al.

Table 1. *Zircon U-Pb isotopic data, North Qaidam orthogneiss samples D7B and D15D*

Analysis	$^{206}Pb_c$ (%)	U (ppm)	Th (ppm)	$^{232}Th/^{238}U$	$^{206}Pb^*$ (ppm)	$^{206}Pb/^{238}U$ Age* (Ma, ±1σ)	$^{207}Pb/^{206}Pb$ Age† (Ma, ±1σ)	disc. (%)	Total $^{238}U/^{206}Pb$ (± % err)	Total $^{207}Pb/^{206}Pb$ (± % err)	$^{207}Pb^*/^{235}U$† (± % err)	$^{206}Pb^*/^{238}U$† (± % err)	err corr
cores													
D7B-2	0.72	945	50	0.05	116.2	856.7 ± 2.5	949 ± 21	10	7.0 ± 0.3	0.0736 ± 0.6	1.3910 ± 1.1	0.1427 ± 0.3	0.276
D7B-5	0.24	610	54	0.09	76.2	873.9 ± 3.4	937 ± 15	7	6.9 ± 0.4	0.0702 ± 0.7	1.4106 ± 0.8	0.1456 ± 0.4	0.472
D7B-6‡	0.02	594	68	0.12	79.7	936.3 ± 10.6	934 ± 20	0	6.4 ± 1.2	0.0705 ± 0.9	1.5130 ± 1.5	0.1563 ± 1.2	0.770
D7B-7‡	0.07	406	54	0.14	54.5	935.0 ± 10.7	927 ± 24	-1	6.4 ± 1.2	0.0708 ± 1.1	1.5049 ± 1.7	0.1560 ± 1.2	0.706
D7B-8‡	--	697	55	0.08	93.9	940.5 ± 10.5	929 ± 18	-1	6.4 ± 1.2	0.0700 ± 0.9	1.5156 ± 1.4	0.1570 ± 1.2	0.798
D7B-9	1.85	522	165	0.33	66.2	872.5 ± 10.1	938 ± 72	7	6.8 ± 1.2	0.0835 ± 0.9	1.4092 ± 3.7	0.1453 ± 1.2	0.321
D7B-12	--	386	42	0.11	51.2	925.8 ± 10.7	879 ± 26	-5	6.5 ± 1.2	0.0698 ± 1.1	1.4526 ± 1.72	0.1541 ± 1.2	0.694
D7B-14‡	--	1093	557	0.53	146.1	932.9 ± 10.2	899 ± 14	-3	6.4 ± 1.1	0.0693 ± 0.6	1.4798 ± 1.3	0.1555 ± 1.1	0.855
D7B-15‡	0.15	629	64	0.11	82.8	918.2 ± 10.3	932 ± 23	1	6.5 ± 1.2	0.0709 ± 1.0	1.4812 ± 1.6	0.1532 ± 1.2	0.726
D7B-16‡	--	932	52	0.06	123.6	926.2 ± 10.2	908 ± 19	-2	6.5 ± 1.1	0.0694 ± 0.9	1.4758 ± 1.5	0.1544 ± 1.1	0.772
D7B-18‡	0.03	1392	94	0.07	184.7	925.5 ± 10.1	919 ± 13	-1	6.5 ± 1.1	0.0702 ± 0.6	1.4832 ± 1.3	0.1544 ± 1.1	0.877
D7B-19‡	--	424	88	0.21	56.8	936.1 ± 10.7	900 ± 22	-4	6.4 ± 1.2	0.0693 ± 1.0	1.4856 ± 1.6	0.1561 ± 1.2	0.750
D7B-20	0.67	849	171	0.21	108.2	885.8 ± 9.9	937 ± 29	6	6.7 ± 1.1	0.0741 ± 0.7	1.4304 ± 1.8	0.1476 ± 1.1	0.627
D7B-21	--	519	63	0.12	68.5	921.5 ± 10.5	893 ± 22	-3	6.5 ± 1.2	0.0693 ± 1.0	1.4559 ± 1.57	0.1535 ± 1.2	0.746
D7B-23	--	493	76	0.16	67.1	950.7 ± 10.8	887 ± 21	-7	6.3 ± 1.2	0.0691 ± 1.0	1.4989 ± 1.54	0.1585 ± 1.2	0.763
D7B-24‡	--	662	102	0.16	89.0	937.9 ± 10.5	926 ± 17	-1	6.4 ± 1.2	0.0701 ± 0.8	1.5088 ± 1.42	0.1565 ± 1.2	0.813
rims													
D7B-3	0.30	175	1	0.00	10.2	420.7 ± 3.4	-- ± --	--	14.8 ± 0.8	0.0576 ± 2.4	0.5469 ± 2.8	0.0677 ± 0.8	0.286
D7B-1	1.38	238	7	0.03	16.3	486.6 ± 6.2	-- ± --	--	12.6 ± 1.3	0.0681 ± 2.0	0.3238 ± 32.6	0.0760 ± 1.7	0.051
D7B-10	0.59	401	14	0.04	34.9	617.5 ± 7.6	756 ± 34	22	9.9 ± 1.2	0.0653 ± 1.4	0.8977 ± 2.06	0.1010 ± 1.3	0.609
D7B-11	3.45	240	14	0.06	13.6	397.2 ± 5.4	-- ± --	--	15.2 ± 1.3	0.0825 ± 2.0	0.3895 ± 19.7	0.0628 ± 1.6	0.080
D7B-13	0.63	395	21	0.05	22.3	408.2 ± 5.0	-- ± --	--	15.2 ± 1.2	0.0600 ± 1.8	0.4879 ± 4.16	0.0653 ± 1.2	0.300
D7B-17	7.68	281	9	0.03	18.4	437.1 ± 7.1	-- ± --	--	13.2 ± 1.3	0.1178 ± 1.6	0.4725 ± 26.7	0.0696 ± 1.7	0.064
D7B-22	0.58	247	2	0.01	16.0	466.4 ± 6.1	-- ± --	--	13.3 ± 1.3	0.0610 ± 2.3	0.5887 ± 3.0	0.0751 ± 1.3	0.439

(continued)

Table 1. (continued)

Analysis	$^{206}Pb_c$ (%)	U (ppm)	Th (ppm)	$^{232}Th/^{238}U$	$^{206}Pb^*$ (ppm)	$^{206}Pb/^{238}U$ Age* (Ma, ±1σ)	$^{207}Pb/^{206}Pb$ Age† (Ma, ±1σ)	disc. (%)	Total $^{238}U/^{206}Pb$ (± % err)	Total $^{207}Pb/^{206}Pb$ (± % err)	$^{207}Pb^*/^{235}U$† (± % err)	$^{206}Pb^*/^{238}U$† (± % err)	err corr
D15D-2	0.15	509	83	0.17	66.5	912.1 ± 3.8	952 ± 17	4	6.6 ± 0.4	0.0707 ± 0.8	1.4867 ± 0.9	0.1522 ± 0.4	0.448
D15D-3	0.06	1370	93	0.07	183.9	935.5 ± 2.3	947 ± 11	1	6.4 ± 0.3	0.0707 ± 0.5	1.5215 ± 0.6	0.1562 ± 0.3	0.437
D15D-4	0.12	322	75	0.24	42.6	921.6 ± 5.2	967 ± 24	5	6.5 ± 0.6	0.0708 ± 1.0	1.5143 ± 1.3	0.1540 ± 0.6	0.447
D15D-1‡	0.10	181	41	0.23	23.2	896.5 ± 11.6	920 ± 38	3	6.7 ± 1.3	0.0698 ± 1.8	1.4356 ± 2.3	0.1493 ± 1.3	0.589
D15D-6	0.51	115	36	0.33	14.6	880.9 ± 13.2	1042 ± 44	18	6.8 ± 1.5	0.0726 ± 2.2	1.5048 ± 2.7	0.1474 ± 1.5	0.576
D15D-7‡	0.14	421	77	0.19	55.0	911.5 ± 10.6	958 ± 23	5	6.6 ± 1.2	0.0706 ± 1.2	1.4899 ± 1.7	0.1522 ± 1.2	0.724
D15D-5	1.09	1418	207	0.15	177.3	866.9 ± 9.6	922 ± 43	6	6.9 ± 1.1	0.0770 ± 0.6	1.3881 ± 2.4	0.1443 ± 1.1	0.480
D15D-8‡	0.05	716	121	0.18	94.4	920.7 ± 10.3	925 ± 18	0	6.5 ± 1.2	0.0702 ± 0.9	1.4796 ± 1.5	0.1536 ± 1.2	0.794
D15D-9‡	--	266	70	0.27	35.7	937.7 ± 11.4	873 ± 30	-7	6.4 ± 1.3	0.0680 ± 1.5	1.4671 ± 1.9	0.1562 ± 1.3	0.652
D15D-10‡	0.14	1143	102	0.09	149.8	913.8 ± 10.1	944 ± 14	3	6.6 ± 1.1	0.0707 ± 0.7	1.4831 ± 1.3	0.1525 ± 1.1	0.857
D15D-11‡	0.24	907	133	0.15	117.4	902.5 ± 10.0	933 ± 19	3	6.6 ± 1.1	0.0711 ± 0.8	1.4553 ± 1.5	0.1505 ± 1.1	0.779
D15D-12‡	--	267	57	0.22	35.0	914.6 ± 11.1	929 ± 29	2	6.6 ± 1.2	0.0695 ± 1.4	1.4727 ± 1.9	0.1525 ± 1.2	0.657
D15D-13	1.90	542	193	0.37	68.9	873.5 ± 10.1	940 ± 77	7	6.8 ± 1.2	0.0840 ± 0.9	1.4124 ± 3.9	0.1455 ± 1.2	0.304
D15D-14‡	0.11	322	98	0.31	41.6	903.1 ± 10.7	926 ± 26	2	6.6 ± 1.2	0.0701 ± 1.3	1.4512 ± 1.8	0.1505 ± 1.2	0.696
D15D-15‡	--	355	86	0.25	46.6	917.3 ± 10.8	914 ± 24	0	6.5 ± 1.2	0.0691 ± 1.2	1.4653 ± 1.7	0.1529 ± 1.2	0.716
D15D-16‡	--	365	160	0.45	48.6	928.8 ± 10.9	934 ± 34	1	6.5 ± 1.2	0.0698 ± 1.7	1.5001 ± 2.1	0.1550 ± 1.2	0.585
D15D-17	1.87	67	34	0.52	25.1	2307.9 ± 35.8	2496 ± 18	6	2.3 ± 1.5	0.1633 ± 1.1	9.9212 ± 1.8	0.4390 ± 1.5	0.802
D15D-18‡	--	646	91	0.15	87.0	938.9 ± 10.6	934 ± 19	0	6.4 ± 1.2	0.0703 ± 0.9	1.5174 ± 1.5	0.1568 ± 1.2	0.780

Note: Abbreviations: Pb_c and Pb^* denote the common and radiogenic portions, respectively; disc., discordance = ($^{207}Pb/^{206}Pb$ Age - $^{206}Pb/^{238}U$ Age)/($^{206}Pb/^{238}U$ Age). Samples were analyzed in two sessions: samples D7B-2, D7B-3, D7B-5, D15D-2, D15D-3, and D15D-4 (not plotted on Fig. 3) were analysed 11 October 2003, for which the error in standard calibration was 0.46% (2σ); all other samples were analyzed 3–4 March 2005, for which the error in standard calibration was 0.66% (2σ). The error in standard calibration is not included in the errors listed above, but is required when comparing data from different sessions, or with other geochronological data.

*Common Pb corrected by assuming $^{206}Pb/^{238}U$ - $^{207}Pb/^{235}U$ age-concordance (^{207}Pb correction, Williams, 1998).

†Common Pb corrected using measured ^{204}Pb.

‡Analysis included in concordia age calculation.

Table 2. *Zircon trace element data, North Qaidam orthogneiss samples D7B and D15D (abundances expressed in ppm).*

sample	CL	La	Ce	Nd	Sm	Eu	Gd	Dy	Er	Yb	Lu	Hf	Th	U	Eu/Eu*	Lu_n/Gd_n
D7B-1	b	2.47	7.42	5.52	3.13	0.33	12.2	102.2	113.2	152.3	25.6	12136	29	904	0.16	17
D7B-2	d	0.32	1.01	1.17	1.43	0.05	14.7	148.0	183.7	226.2	34.5	11882	51	1559	0.03	19
D7B-3	b	0.11	0.27	0.25	0.15	0.04	0.9	8.8	8.9	13.2	2.4	12291	1	328	0.33	22
D7B-4	o	0.01	0.61	1.11	1.77	0.04	15.8	122.3	252.4	524.0	107.4	9373	30	268	0.02	55
D7B-5	o	0.04	0.47	0.84	1.58	0.03	16.7	154.3	285.6	546.0	104.8	10087	45	792	0.02	51
D15D-1	o	0.13	1.16	1.31	1.75	0.11	13.5	75.0	138.9	302.0	66.0	10100	44	327	0.07	39
D15D-2	o	0.03	1.23	1.10	1.69	0.09	13.8	85.6	163.1	344.3	71.4	9427	57	538	0.06	42
D15D-3	d	0.19	1.57	1.20	1.67	0.09	15.3	132.3	309.9	765.6	167.4	10487	73	1509	0.06	88
D15D-4	o	0.01	0.91	1.62	2.46	0.17	17.1	60.3	58.0	84.9	15.6	8849	42	255	0.08	7
D15D-5	o	22.43	94.95	52.22	28.50	3.02	75.1	277.8	366.6	793.7	170.0	10336	171	1624	0.20	18

Note: Analyses performed 12 - 13 August 2003. Eu/Eu* = $Eu_n/(Sm_n * Gd_n)^{0.5}$; the subscript indicates normalization to chondrite values of McDonough and Sun (1995). Abbreviations: b, bright CL; d, dark CL; o, oscillatory CL zoning.